Structural insights into the Ca^{2+} and $PI(4,5)P_2$ binding modes of the C2 domains of rabphilin 3A and synaptotagmin 1

Jaime Guillén[a], Cristina Ferrer-Orta[b], Mònica Buxaderas[b], Dolores Pérez-Sánchez[a], Marta Guerrero-Valero[a], Ginés Luengo-Gil[a], Joan Pous[b,c], Pablo Guerra[b], Juan C. Gómez-Fernández[a], Nuria Verdaguer[b,1], and Senena Corbalán-García[a,1]

[a]Departamento de Bioquímica y Biología Molecular A, Facultad de Veterinaria, Regional Campus of International Excellence "Campus Mare Nostrum," Universidad de Murcia, 30100 Murcia, Spain; [b]Instituto de Biología Molecular de Barcelona, Consejo Superior de Investigaciones Cientificas, 08028 Barcelona, Spain; and [c]Institute for Research in Biomedicine, Parc Científic de Barcelona, 08028 Barcelona, Spain

Edited by Axel T. Brunger, Stanford University, Stanford, CA, and approved November 14, 2013 (received for review August 27, 2013)

Proteins containing C2 domains are the sensors for Ca^{2+} and PI(4,5)P_2 in a myriad of secretory pathways. Here, the use of a free-mounting system has enabled us to capture an intermediate state of Ca^{2+} binding to the C2A domain of rabphilin 3A that suggests a different mechanism of ion interaction. We have also determined the structure of this domain in complex with PI(4,5)P_2 and IP_3 at resolutions of 1.75 and 1.9 Å, respectively, unveiling that the polybasic cluster formed by strands β3–β4 is involved in the interaction with the phosphoinositides. A comparative study demonstrates that the C2A domain is highly specific for PI(4,5)P_2/PI(3,4,5)P_3, whereas the C2B domain cannot discriminate among any of the diphosphorylated forms. Structural comparisons between C2A domains of rabphilin 3A and synaptotagmin 1 indicated the presence of a key glutamic residue in the polybasic cluster of synaptotagmin 1 that abolishes the interaction with PI(4,5)P_2. Together, these results provide a structural explanation for the ability of different C2 domains to pull plasma and vesicle membranes close together in a Ca^{2+}-dependent manner and reveal how this family of proteins can use subtle structural changes to modulate their sensitivity and specificity to various cellular signals.

PIP2 | calcium | vesicle fusion

C2 modules are most commonly found in enzymes involved in lipid modifications and signal transduction and in proteins involved in membrane trafficking. They consist of 130 residues and share a common fold composed of two four-stranded β-sheets arranged in a compact β-sandwich connected by surface loops and helices (1–4). Many of these C2 domains have been demonstrated to function in a Ca^{2+}-dependent membrane-binding manner and hence act as cellular Ca^{2+} sensors. Calcium ions bind in a cup-shaped invagination formed by three loops at one tip of the β-sandwich where the coordination spheres for the Ca^{2+} ions are incomplete (5–7). This incomplete coordination sphere can be occupied by neutral and anionic (7–9) phospholipids, enabling the C2 domain to dock at the membrane.

Previous work in our laboratory has shed light on the 3D structure of the C2 domain of PKCα in complex with both PS and $PI(4,5)P_2$ simultaneously (10). This revealed an additional lipid-binding site located in the polybasic region formed by β3–β4 strands that preferentially binds to $PI(4,5)P_2$ (11–15). This site is also conserved in a wide variety of C2 domains of topology I, for example synaptotagmins, rabphilin 3A, DOC2, and PI3KC2α (10, 16–19). Given the importance of $PI(4,5)P_2$ for bringing the vesicle and plasma membranes together before exocytosis to ensure rapid and efficient fusion upon calcium influx (20–23), it is crucial to understand the molecular mechanisms beneath this event.

Many studies have reported different and contradictory results about the membrane binding properties of C2A and C2B domains of synaptotagmin 1 and rabphilin 3A providing an unclear picture about how Ca^{2+} and $PI(4,5)P_2$ combine to orchestrate the vesicle fusion and repriming processes by acting through the two C2 domains existing in each of these proteins (16, 20, 22, 24–28). A myriad of works have explored the 3D structure of the individual C2 domains of both synaptotagmins and rabphilin 3A (5, 26, 27, 29, 30). However, the impossibility of obtaining crystal structures of these domains in complex with Ca^{2+} and phosphoinositides has hindered the understanding of the molecular mechanism driving the $PI(4,5)P_2$–C2 domain interaction. Here, we sought to unravel the molecular mechanism of Ca^{2+} and $PI(4,5)P_2$ binding to the C2A domain of rabphilin 3A by X-ray crystallography. A combination of site-directed mutagenesis together with isothermal titration calorimetry (ITC), fluorescence resonance of energy transfer (FRET), and aggregation experiments has enabled us to propose a molecular mechanism of Ca^{2+}/$PI(4,5)P_2$-dependent membrane interaction through two different motifs that could bend the membrane and accelerate the vesicle fusion process. A comparative analysis revealed the structural basis for the different phosphoinositide affinities of C2A and -B domains. Furthermore, the C2A domain of synaptotagmin 1 lacks one of the key residues responsible for the $PI(4,5)P_2$ interaction, confirming it is a non-PI(4,5)P_2 responder.

Significance

Vesicle fusion is an important event in neuronal transmission and endocrine cell secretion. A myriad of proteins containing double C2 domains are involved in this complex process; however, how Ca^{2+} and the different types of membrane lipids regulate their function is still not well understood. In this work, we provide structural insights to explain the ability of different C2 domains to interact with Ca^{2+} and PI(4,5)P_2 and demonstrate the existence of a specific PI(4,5)P_2-binding motif that provides these domains with specific properties to interact with the membrane and initiate vesicle fusion. We also demonstrate a unique molecular mechanism conferring their specificity for the different phosphoinositides, which resides in additional amino acidic residues surrounding the key interacting lysines.

Author contributions: N.V. and S.C.-G. designed research; J.G., C.F.-O., M.B., D.P.-S., M.G.-V., G.L.-G., J.P., and P.G. performed research; J.G., C.F.-O., M.B., D.P.-S., J.P., P.G., J.C.G.-F., N.V., and S.C.-G. analyzed data; and N.V. and S.C.-G. wrote the paper.

The authors declare no conflict of interest.

This article is a PNAS Direct Submission.

Data deposition: The atomic coordinates and structure factors have been deposited in the Protein Data Bank, www.pdb.org [PDB ID codes 4LT7 (C2A-Ca^{2+}), 4NP9 (C2A-IP3), and 4NS0 (C2A+PIP2)].

[1]To whom correspondence may be addressed. E-mail: senena@um.es or nvmcri@ibmb.csic.es.

This article contains supporting information online at www.pnas.org/lookup/suppl/doi:10.1073/pnas.1316179110/-/DCSupplemental.

Results and Discussion

A Different Ca^{2+}-Binding Mechanism for the C2A Domain of Rabphilin 3A. Despite the different cocrystallization conditions tested (*SI Appendix*, *SI Methods*), all attempts addressed at obtaining the calcium-bound form of the C2A domain of rabphilin 3A in crystals failed. To overcome this problem of low Ca^{2+} affinity (1.1 mM, determined by NMR at pH 7.0) (27), we used a free-mounting system (FMS) (31), installed in an in-house rotating anode generator to test whether fine control of the relative humidity (RH) could be used to optimize the soaking conditions with Ca^{2+}. At 99% of relative humidity, the unit cell of rabphilin C2A crystals was expanded by 5% and this was sufficient to allow the small structural rearrangements required to introduce one Ca^{2+} ion into the unbound crystals. A new adjustment of the relative humidity to the optimum, 96%, allowed us to collect a complete data set (2.5-Å resolution) after the soaking (*Materials and Methods* and *SI Appendix*, Table S1). Initial maps, after rigid body fitting of the C2A coordinates to the new cell, showed the presence of a strong peak of electron density that would correspond to the presence of a Ca^{2+} ion bound to the calcium-binding region (CBR) of the domain. Small rearrangements in the region, in particular in CBR3, were also visible (Fig. 1 *A* and *B*). The Ca^{2+} ion contacts the acidic side chains of residues Asp413 of CBR1 and Asp476 and Glu482 of CBR3 but maintaining an incomplete coordination. Strikingly, this ion was located close to the conventional position of Ca2 described for most of the Ca^{2+}-dependent C2 domains (2, 5, 32), indicating the existence of an intermediate step in the calcium-binding process. Thus, we compared both the 3D structures and electrostatic potentials of the Ca^{2+}-free (Protein Data Bank, PDB ID code 2CHD) (29) and the $2Ca^{2+}$-bound structures (PDB ID code 2K3H) (27) with the structure determined in this work.

Significant changes were observed within the CBR1 and CBR3 regions (*SI Appendix*, Fig. S1). In the Ca^{2+}-free form, the orientation of these residues was incompatible with Ca^{2+} coordination (*SI Appendix*, Fig. S1*A*), leading to a very narrow space between CBR1 and CBR3 (named "closed conformation") that impedes Ca^{2+} access through the top of the domain (*SI Appendix*, Fig. S1*D*). The only way for Ca^{2+} to interact is by two exposed electronegative cavities at each lateral side of the CBR (*SI Appendix*, Fig. S1*D*). On the right, Asp413, Asp476, and Glu482 contribute to form the electronegative area (*SI Appendix*, Fig. S1 *A* and *D*) and in the $1Ca^{2+}$-bound form, Asp476 moves down to coordinate the Ca^{2+} ion together with the other two aspartate residues (*SI Appendix*, Fig. S1 *B* and *E*). In this intermediate state the bound Ca^{2+} is not still in position P2. A further reorganization, consisting of an ∼2-Å movement of main and side chains of D413, is needed to allow the accommodation of the Ca^{2+} ion into its final P2 position. However, this movement does not explain the large conformational change needed to open the CBR, as seen in the two Ca^{2+}-bound structure (*SI Appendix*, Fig. S1 *C* and *F*) (27).

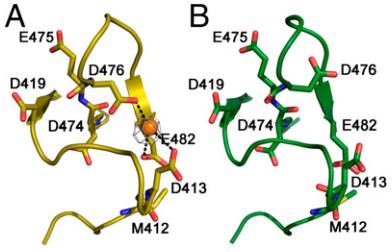

Fig. 1. Structure of rabphilin 3A–C2A domain bound to Ca^{2+}. Ribbon diagrams of the calcium-binding region in the one Ca^{2+} bound (*A*; yellow) and unbound (*B*; green) C2A structures. The five critical Asp residues involved in Ca^{2+} coordination are represented by sticks. Coordination interactions are represented by dashed black lines. The initial weighted |Fo|-|Fc| electron density map (contoured at 3.5 σ) calculated in absence of the Ca^{2+} ion is shown as dark blue mesh around the ligand molecule.

Unfortunately, in our crystals, the left cavity (formed by residues Asp419 and Glu475) is not accessible, due to an intermolecular salt bridge formed between Asp419 and Arg503 in the crystal packing. The $2Ca^{2+}$-bound conformation (named "open conformation") shows that side chains of Asp476 and Asp413 are displaced to the left to coordinate the Ca^{2+} ion of position P1 (Ca1), resulting in the conformational change that opens the cavity (*SI Appendix*, Fig. S1 *C* and *F*) and explaining how this domain overcomes the high activation energy barrier needed to adopt the final open conformation. However, we cannot completely rule out the possibilities of a sequential binding, implying a Ca^{2+} movement from the right intermediate site to the left or a simultaneous binding by two Ca^{2+} entries through each of the sites.

The need of this large rearrangement in the CBRs of rabphilin C2A domain might explain the low Ca^{2+} affinity exhibited by this domain in the absence of membranes, but does not provide information about the mechanism by which the domain adopts the incompatible Ca^{2+} binding closed conformation, which so far has not been described for any other C2 domain (5). Taking into account that there is no conformational change upon Ca^{2+} binding for the C2A domain of syt1 (5, 33), we compared it with the C2A domain of rabphilin 3A in the absence of Ca^{2+} to find the molecular mechanism that enables rabphilin to adopt these two different conformational states. Three critical differences could be detected: first Pro411 in rabphilin 3A is located one position further than Pro169 in syt1, facilitating in the former the orientation of the CBR1 in the proximity of the CBR3 (Fig. 2*A*). Second, whereas the side chain of Arg445 in the CBR2 of rabphilin 3A strongly interacts with Pro411, contributing to maintaining the CBR1 orientation close to the CBR3, it is in fact substituted by Leu202 in syt1 (Fig. 2*A*). Third, the salt bridge between Glu475 in the aspartic–glutamic–aspartic motif of rabphilin 3A and Arg437 (β4 strand) (27) is not conserved in syt1, thus leaving its CBR3 more flexible to adopt the conformation compatible with Ca^{2+} binding (Fig. 2*B*). The reason why rabphilin 3A specifically needs this conformational change upon Ca^{2+} binding is not known but this protein is a Rab3/Rab27 effector in neurons and endocrine cells (reviewed in refs. 34, 35), and is involved in vesicle docking and repriming (36, 37). This implies it has to be present in scenarios with concomitant Ca^{2+} influx that triggers vesicle fusion through its main target syt1. In this way, the low Ca^{2+} affinity of the C2A domain of rabphilin 3A would convert it into a perfect candidate to be located at the fusion area without competing with syt1, but being ready for repriming immediately after vesicle fusion occurs.

Comparison of the three conformational states of the C2A domain of rabphilin 3A showed that the main change occurs when two Ca^{2+} are bound to the domain leading to the unleashing of the Arg437/Glu475 interaction and a large displacement of the side chain of Arg445 to the protein surface that also prevents the interaction with Pro411 (*SI Appendix*, Fig. S2 *A* and *B*). Primary sequence alignment of these regions revealed that only the C2A domain of rabphilin 3A conserves these four residues (*SI Appendix*, Fig. S2*C*). The C2A domains of DOC2B and DOC2A conserve some of the residues (*SI Appendix*, Fig. S2*C*), making difficult to predict whether these domains might adopt the closed or open conformation without further experimentation. However, it is clear that the similarity of DOC2B to rabphilin 3A is higher than to syt1, and this might explain the different behaviors found for it in recent studies using KO mice (38–40).

Three Dimensional Structure of Rabphilin–C2A in Complex with IP_3 and $PI(4,5)P_2$ Confirms the Existence of a Specific Phosphoinositide-Binding Site in Some C2 Domains. The recombinant rabphilin–C2A domain was also crystallized in the presence of IP_3-Ca^{2+} and PI(4,5)P_2-Ca^{2+} (*SI Appendix*, Table S1 and *SI Methods*). The X-ray structures were determined at 1.9 Å and 1.75 Å for the IP_3 and PI(4,5)P_2, respectively (*SI Appendix*, Table S1). Surprisingly, the analysis of the electron density maps did not show ordered Ca^{2+} densities in the calcium-binding regions in any of the complexes analyzed. In contrast, well-defined extra electron densities were

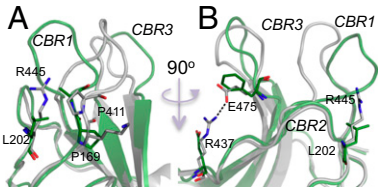

Fig. 2. Three dimensional comparison of C2A domain structures of Ca^{2+}-free rabphilin 3A and syt1. (*A*) Three dimensional overlap of Cα of the C2 domains from rabphilin 3A (PDB ID code 2CHD, gray) and syt1 (PDB ID code 1RSY, green). Sticks represent the side chains of the critical residues involved in the different conformational changes. (*B*) Similar representation turned 90° to the right.

found within the concave surface of the C2A domain, in the two complexes. These densities were explained by the presence of the phospholipid ligands bound to the polybasic region formed by the strands β3–β4 of the domain (Fig. 3 *A* and *B* and *SI Appendix*, Fig. S3 *A* and *B*). A strong peak of extra electron density in the vicinity was interpreted by the presence of a sulfate ion from the crystallization solution, also occupying the cavity and interacting with the side chains of three residues, Arg469 and Lys423 of strand β6 and Arg422, coming from a neighboring C2A domain in the crystal packing (Fig. 3*B*).

The root mean square deviation (rmsd) of the superimpositions of all equivalent Cα atoms from the isolated C2A domain (PDB ID code 2CHD) with those of the two complexes are 0.12 Å and 0.18 Å for the IP_3 and $PI(4,5)P_2$ ligands, respectively, indicating that the two structures are essentially identical. Lys423 of strand β3 forms a double salt bridge with phosphate 4; Lys435 of strand β4 forms a hydrogen bond with the hydroxyl group O3 of the inositol; and Arg437, within β4, contacts the phosphate 5 moiety. Note that this residue is also involved in the interaction with Glu475 in the absence of Ca^{2+}, suggesting a pivotal role for the arginine residue in the activation of rabphilin 3A by Ca^{2+} and $PI(4,5)P_2$. Phosphates 4 and 5 appear also hydrogen bonded to Tyr421 of β3 and Asn481 of CBR3. Finally, phosphate 5 forms an additional salt bridge with the side chain of Lys410, which belongs to a neighboring C2A domain in the crystal (Fig. 3 *A* and *B* and *SI Appendix*, Fig. S3). The final refined maps of the C2A–$PI(4,5)P_2$ complex show well-defined electron density that allows the positioning of part of the fatty acyl chains of the phospholipid, occupying a cavity formed at the contact interface between two neighboring C2A domains in the crystal packing.

Ca^{2+} and $PI(4,5)P_2$ Cooperate to Increase the Affinity of the C2 Domains of Rabphilin 3A to Bind to Membranes Through the Lysine-Rich Cluster. The crystallographic data suggest that this particular C2A domain might interact with $PI(4,5)P_2$ through the lysine-rich cluster region independently of Ca^{2+}. We compared the membrane-binding properties of the C2A and C2B domains of rabphilin 3A by using protein-to-membrane FRET (41, 42). Ca^{2+} increased the affinity of both C2A and C2B domains to bind lipid vesicles containing both 1-palmitoyl-2-oleoyl-sn-glycero-3-phospho-L-serine (POPS) and $PI(4,5)P_2$ (Fig. 4 *A* and *B* and *SI Appendix*, Table S2). Further exploration of the thermodynamic parameters (ITC) of liposome binding to the C2A domain in the presence of Ca^{2+} demonstrated that a combination of POPS and $PI(4,5)P_2$ in the membranes renders the higher binding affinity and suggests that one molecule of phosphoinositide might bind per domain (*SI Appendix*, Fig. S4 *A–D* and Table S3). Strikingly, the binding reaction for the C2B domain was endothermic with slightly lower binding affinity than the C2A domain (*SI Appendix*, Fig. S4*E* and Table S3).

To confirm the role of the residues involved in $PI(4,5)P_2$-dependent binding, we substituted Lys423 or Lys435/Arg437 in the C2A domain and Lys581 or Lys593/Lys595 in the C2B domain by Ala. FRET membrane binding demonstrated that both domains lost their ability to interact with 1-palmitoyl-2-oleoyl-sn-glycero-3-phosphocholine (POPC)/POPS/$PI(4,5)P_2$ liposomes (Fig. 4 *C* and *D*), confirming the role of the polybasic patch in the $PI(4,5)P_2$-specific interaction in these two domains.

Our work corroborates that Ca^{2+} increases the affinity of the C2A and C2B domains of rabphilin 3A to bind $PI(4,5)P_2$-containing membranes (25, 28). However, our crystallographic data strongly suggest that in the absence of Ca^{2+}, at least the C2A domain might interact with membranes enriched in $PI(4,5)P_2$ using the phosphoinositide as an anchor to specific areas of the plasma membrane (43) (through the lysine-rich cluster interaction). In a second step, Ca^{2+} influx would facilitate a second interaction with phosphatidylserine (through the CBR), forcing the domain to dock in the membrane through two different points that now will distort the curvature as a consequence (Fig. 5 *A* and *B*).

C2A and C2B Domains of Rabphilin 3A Differentially Interact with Other Phosphoinositides. We also studied the phosphoinositide-specificity profile of these C2 domains. Both domains exhibited similar affinity to bind $PI(3,4,5)P_3$- and $PI(4,5)P_2$- containing vesicles (*SI Appendix*, Table S2). A model docking of $PI(3,4,5)P_3$ on the β3–β4 grooves of C2A showed that phosphate 3 can be easily accommodated into the pocket in close contact with the basic residues His425 and Lys435 (*SI Appendix*, Fig. S5 *A* and *B*).

Modeling of the $PI(4,5)P_2$ and $PI(3,4,5)P_3$ molecules in the lysine-rich cluster of the C2B domain showed that they are able to interact with the three homolog lysine residues (Lys581, Lys593, and Lys595) and Asn638 (*SI Appendix*, Fig. S5 *C* and *D*). However, a Phe (Phe579) residue appears instead of a Tyr, indicating this might be the reason for the slightly lower binding affinity and endothermic nature of the membrane interaction observed by ITC. Furthermore, His425 in C2A is a Trp in C2B, which hampers the interaction with phosphate 3. Strikingly, these two residues do not seem to be critical for the $PI(4,5)P_2$/$PI(3,4,5)P_3$-dependent interaction of the C2B domain but rather influence the thermodynamic nature of the membrane association.

Interestingly, the C2A domain showed very low binding affinity with mixtures containing $PI(3,4)P_2$ and $PI(3,5)P_2$ (*SI Appendix*, Table S2). On the contrary, the C2B domain did not discriminate among the double phosphorylated phosphoinositides (*SI Appendix*, Table S2) showing a lower degree of specificity. Taking into account the structural models proposed for $PI(3,4,5)P_3$ and $PI(4,5)P_2$ interactions for the C2A and C2B domains (*SI Appendix*, Fig. S5), the C2A domain keeps only 55–66% of binding capacity, whereas the C2B domain still keeps 71–86% in the cases of $PI(3,4)P_2$ and $PI(3,5)P_2$. This fits very well with the biochemical results obtained (*SI Appendix*, Table S4), suggesting that the lower number of interactions established by the C2B

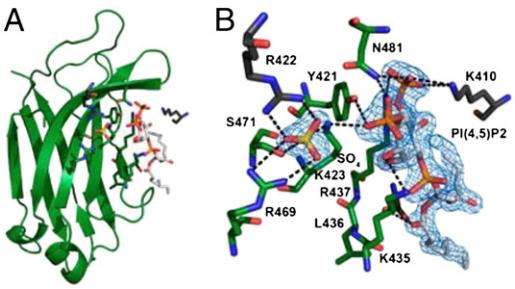

Fig. 3. Structure of rabphilin C2A domain bound to $PI(4,5)P_2$. (*A*) The C2A–$PI(4,5)P_2$ complex. The C2A molecule is shown in green with the side chains of amino acids within the β3–β4 groove, directly interacting with the phospholipid depicted as sticks. The phosphate ions and phospholipid molecule are shown as sticks in atom type color. (*B*, *Right*) Close-up view of the β3–β4 groove, indicating the interactions between the C2A domain and the $PI(4,5)P_2$ ligand. The C2A contacting residues and the corresponding ligands are represented in sticks and explicitly labeled. Hydrogen bonds are shown as dashed lines in black. The weighted 2|Fo|-|Fc| electron density map (contoured at 1.5 σ) is shown as blue mesh around the ligand molecule.

BIOCHEMISTRY

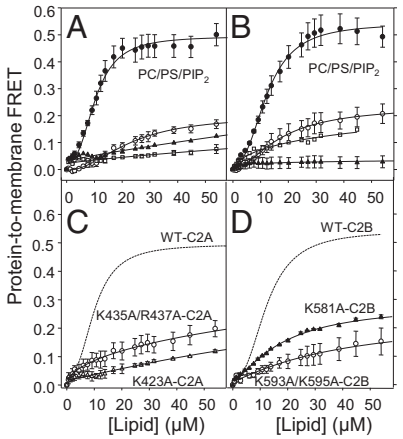

Fig. 4. Binding of C2A (*A*) and C2B (*B*) domains of rabphilin 3A assessed by protein-to-membrane FRET. Small unilamellar vesicles (SUVs) composed of POPC/POPS/PI(4,5)P_2/N-(5-dimethylaminonaphthalene-1-sulfonyl)-1,2-dihexadecanoyl-sn-glycero-3-phosphoethanolamine (dDHPE) (molar ratio 65:25:5:5) (●,▲), POPC/PI(4,5)P2/dDHPE (molar ratio 90:5:5) (○), and POPC/POPS/dDHPE (molar ratio 70:25:5) (□) were titrated into a solution containing 0.8 μM of C2 domains in the presence of 100 μM $CaCl_2$ (●) or 1 mM EGTA (▲). A 57% correction was used to calculate the PI(4,5)P_2 or POPS available for C2 domain binding. Effect of mutations K423A and K435A/R437A in the C2A domain (*C*) and K581A and K593A/K595A in the C2B domain (*D*) on lipid binding. Data correspond to titrations of SUVs composed of POPC/POPS/PI(4,5)P_2/dDHPE (molar ratio 70:25:5:5) into solutions containing 0.8 μM of wild-type C2 domains (●), C2A (K423A) (Δ), C2A (K435A/R437A) and C2B (K593A/K595A) (○), and C2B (K581A) (▲).

domain, together with the higher electropositive potential in its phosphoinositide-binding cavity and surrounding area (*SI Appendix*, Fig. S6) contribute to decrease its PI(4,5)P_2 specificity. These results reveal a very sophisticated mechanism for the C2 domains to respond to phosphoinositides: first, a collection of three basic residues are essential to hold the phosphoinositide ring (K423, K435, and R437 in C2A); and second, several residues in the surrounding area determine the specificity for each particular phosphoinositide, and the higher number of interactions implies a higher specificity.

The Different PI(4,5)P_2-Binding Properties of the C2A Domain of Synaptotagmin 1 Are Due to a Single Aspartate Residue Located in the β4 Strand. The structural comparison of the polybasic regions of the C2A domains of rabphilin 3A and syt1 allowed the detection of a striking change in the sequence of these domains: Arg437 in rabphilin 3A is substituted by Glu194 in syt1 (*SI Appendix*, Fig. S7*A*), suggesting that this change might affect the ability of the C2A domain of syt1 to interact with PI(4,5)P_2. Thus, we studied the binding properties of the wild-type C2A and C2B domains of syt1. The thermodynamic parameters, calculated for the syt1–C2B domain using POPC/POPS/PI(4,5)P_2 membranes as a ligand, showed one molecule of lipid and a very high affinity (*SI Appendix*, Table S3 and Fig. S7*C*). The C2A domain exhibited lower affinity than the C2B domain for this lipid mixture and did not reach saturation (*SI Appendix*, Table S3 and Fig. S7*B*). Very similar results were obtained by FRET-membrane binding experiments (*SI Appendix*, Table S5 and Fig. S8), showing that the C2A domain exhibits a higher affinity for membranes composed of POPS (*SI Appendix*, Table S5) (44). Mutation of Glu194 to Lys converted the C2A domain in a PI(4,5)P_2-binding module (*SI Appendix*, Fig. S7*D* and Table S3) that was also confirmed by FRET analysis (*SI Appendix*, Fig. S8 and Table S5). Note that the syt1–E194K mutant is a hybrid domain in the sense that it now binds PI(4,5)P_2 like the C2B domain, but still binds POPS like the original C2A domain (*SI Appendix*, Table S5).

The PI(4,5)P_2-Binding Site Confers Upon C2 Domains the Ability to Induce Ca^{2+}-Dependent Vesicle Clustering. Several studies have demonstrated that the C2B domain of syt1 induces Ca^{2+}-dependent lipid aggregation as indicative of the predisposition to facilitate the fusion of synaptic membranes in cooperation with the SNARE complex (19, 45, 46). Critical Arg residues located at the polybasic region (Lys326/Lys327) and at the bottom face (Arg398/Arg399) of the domain are responsible for that function (19, 45, 47). To investigate if the reconstitution of the lysine-rich cluster in the C2A domain of synaptotagmin would participate in this process, we measured the ability of syt1 C2A, syt1 C2A–E194K, and syt1 C2B domains to induce vesicle clustering at increasing protein concentrations. As expected, the C2B domain was able to induce vesicle clustering in a Ca^{2+}/PI(4,5)P_2-dependent manner (Fig. 6*B*), whereas the C2A was not (Fig. 6*A*). Note that for the C2B domain, there was a Ca^{2+}-independent component that at maximum protein concentration represented 50% of the aggregation capacity, indicating that at least two motifs in the domain can cluster lipid vesicles independently of Ca^{2+}, i.e., the lysine-rich cluster and the arginines at the bottom face (Fig. 6*B*) (19, 47, 48). Interestingly, the C2A–E194K mutant recovered the Ca^{2+}-dependent ability to induce aggregation mainly in the presence of POPS/PI(4,5)P_2 (Fig. 6*C*), indicating that once the lysine-rich cluster is reestablished, the domain might interact with lipid vesicles in a way that now induces aggregation.

We also explored whether the polybasic patches of C2A and C2B domains of rabphilin 3A were involved in vesicle aggregation. Mutation in the C2A domain (K435A/R437A) reduced the aggregation to a level similar to that obtained in the absence of Ca^{2+} (Fig. 6*D*), indicating that at least three motifs are involved in the process, similarly to the C2B domain of syt1. Mutations in the C2B domain (K593A/K595A) abolished 50% of the aggregation in the presence of $CaCl_2$ and 90% in its absence (Fig. 6*E*), confirming the role of the polybasic cluster in this process and demonstrating that still two more regions are involved (Fig. 6*E*). Together, these data demonstrate that the polybasic cluster region is essential in the aggregation process, providing C2 domains with the ability of crosslinking secretory vesicles with PI(4,5)P_2/PI(3,4,5)

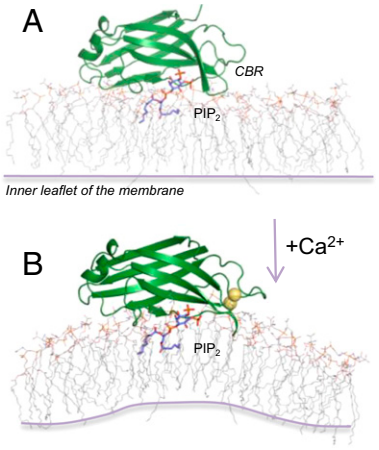

Fig. 5. Docking model of the C2A domain of rabphilin 3A on the membrane surface. The Ca^{2+}-free C2A–PI(4,5)P_2 complex determined in this work was docked on the membrane (*A*). To simulate the two Ca^{2+}-bound forms, we used the PDB ID code 2K3H structure and the PI(4,5)P_2 molecule was added assuming the information obtained in this work (*B*). The model membrane corresponds to a POPC molecular dynamic simulation with PDB ID code popc128a. Half of the bilayer is represented by thin sticks. Take into account that the C2A–PI(4,5)P_2 complex was docked on the lipid bilayer based on the crystal structure solved in this work. Due to the rotation capacity of the different moieties of the phospholipid, including phosphate 1, the acyl chains might adopt different orientations with respect to the phosphoinositide ring, mainly depending on the restrictions imposed by the membrane dynamic and this might also influence the docking orientation of the domain.

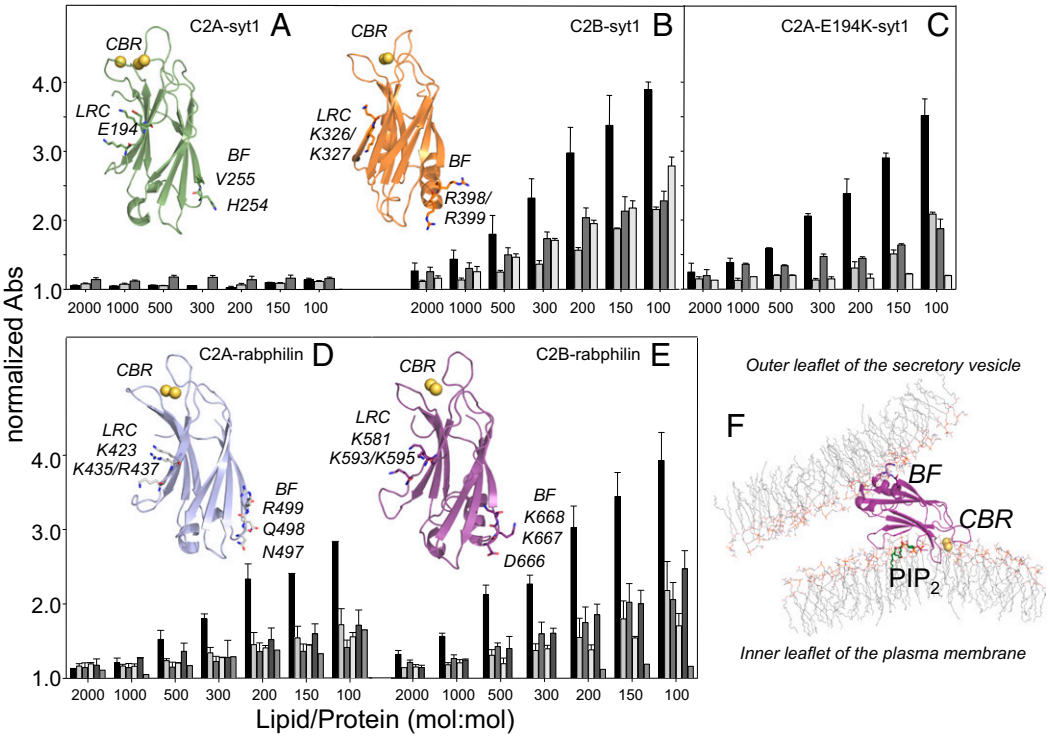

Fig. 6. Effect of PI(4,5)P_2 on the induction of aggregation of C2A and C2B domains of syt1 and rabphilin 3A. SUVs (0.27 mM) of different composition [POPC/POPS/PI(4,5)P_2, POPC/POPS, EGTA-POPC/POPS/PI(4,5)P_2 for C2A and POPC/POPS/PI(4,5)P_2, POPC/PI(4,5)P_2, POPC/POPS, EGTA-POPC/POPS/PI(4,5)P_2 for C2B and C2A–E194K, from *Left* to *Right* in each group of the figure] were incubated with increasing concentration of syt1 C2A (*A*), C2B (*B*), or C2A–E194K (*C*) domains. The same concentrations of SUV of different compositions were incubated with increasing rabphilin 3A: C2A [POPC/POPS/PI(4,5)P_2, POPC/PI(4,5)P_2, POPC/POPS, EGTA-POPC/POPS/PI(4,5)P_2, K435A/R437A-POPC/POPS/PI(4,5)P_2 EGTA-K435A/R437A-POPC/POPS/PI(4,5)P_2 (*D*)] or C2B [POPC/POPS/PI(4,5)P_2, POPC/PI(4,5)P_2, POPC/POPS, EGTA-POPC/POPS/PI(4,5)P_2, K593A/K595A-POPC/POPS/PI(4,5)P_2, EGTA-K593A/K595A-POPC/POPS/PI(4,5)P_2 (*E*)] domains. The increment in Abs at 405 nm was measured after 30 min at 25 °C. Cartoons corresponding to the 3D structures of C2A and C2B domains of syt1 (PDB ID codes 1BYN and 1K5W, respectively) and C2A and C2B domains of rabphilin 3A (PDB ID codes 2K3H and 3RPB, respectively) with the bound Ca^{2+} ions shown as yellow spheres and the side chains of critical basic and acidic residues represented as sticks. CBR, lysine-rich cluster (LRC) and bottom face (BF) are also indicated. (*F*) Model for membrane crosslinking by the C2B domain of rabphilin 3A. The model membranes correspond to a POPC molecular dynamic simulation with PDB code popc128a; they have been oriented to represent a secretory/synaptic vesicle about 40 nm in diameter (*Top*) and the bended plasma membrane by the simultaneous PI(4,5)P_2/Ca^{2+} interaction as explained in Fig. 5 *A* and *B*.

P_3-enriched areas of the plasma membrane. Given the close proximity of the lysine-rich cluster and the CBR, these results are compatible with a parallel orientation model (Fig. 6*F*) in which these two motifs would interact with a vesicle representing the plasma membrane, leaving the bottom face free to interact *in trans* with another lipid vesicle (19, 47–51). How these two C2 domains act in tandem and in cooperation with other SNARE proteins to regulate vesicle fusion is still under debate and will need further exploration.

Conclusions

In the present work we determined the 3D structure of an intermediate state of the C2A domain of rabphilin 3A, which suggests a unique mechanism of Ca^{2+} binding for this particular C2 domain and explains the conformational changes observed between the Ca^{2+}-free and -bound forms. This work also revealed the molecular mechanism underlying the PI(4,5)P_2 interaction with the different C2 domains of both rabphilin 3A and syt1 and demonstrates that the specificity to bind other phosphoinositides resides in the residues surrounding the basic cluster. The results obtained with the C2A domain of syt1 clearly prove that it has lost one of the key lysine residues in the cluster and is no longer capable of binding the phosphoinositide. The general scenario that is emerging is that a wide variety of C2 domain-containing proteins work as an integration platform for a number of different signals. Their activity is coordinated and finely tuned through their capacity to respond differently to a series of subtle changes in Ca^{2+} and phosphoinositides through their CBR and lysine-rich cluster. For example, rabphilin 3A can respond to PI(4,5)P_2 and PI(3,4,5)P_3 through its C2A domain, while recognizing other diphosphorylated forms by means of its C2B domain, and has a very slow response to Ca^{2+}. On the contrary, syt1 is a fast Ca^{2+} sensor but its C2A domain cannot respond specifically to any phosphoinositide through the lysine-rich cluster; however, it recognizes PI(4,5)P_2 with very high affinity by its C2B domain. This also supports the idea that a precise positioning of the Lys residues in the β3–β4 strands of a C2 domain can determine its ability to interact with phosphoinositides specifically, which is a key step in the localization mechanism and probably in the triggering of vesicle fusion. In general, all these observations fit into the idea that individual fusion areas might contain mixtures of fast and slow Ca^{2+} sensors that together with high and low specific PI(4,5)P_2 sensors can efficiently respond to the myriads of functions to cover in these restricted areas.

Materials and Methods

Preparation of the Rabphilin 3A C2A-Ca^{2+} Complex by Soaking, with the FMS. As both, cocrystallization and soaking experiments failed to introduce Ca^{2+} ions into the Rabphilin 3A C2A crystals, we explored a unique soaking protocol, using a FMS adapted and installed in a Rigaku rotating anode X-ray generator (31). The experimentally determined RH equilibrium of the mother liquor of the C2A crystals (52) (96%) was used as the starting point for the experiment. The crystal was mounted in the air stream using a mesh loop and an initial diffraction image was taken to evaluate the diffraction quality of the crystal and determine the initial lattice parameters. Then the crystal was subjected to a controlled variation of the RH, checking both RH increment (from 96% to 99%) and reduction (from

96% to 80%), in steps of 0.5% with an equilibration period of 10 min. In every step, the unit cell parameters were recalculated and the diffraction quality was visually checked, achieving the best diffraction pattern at 96% RH. At 99% of RH, a significant increment of the unit volume (~5%) was observed. At this point an "in situ" soaking experiment was performed as follow: the soaking solution, containing 0.1 M $CaCl_2$, 25 mM Hepes pH 7.6 and 25% (wt/vol) PEG was harvested in a nylon loop (0.05 mm) that was carefully attached to the crystal as shown in (*SI Appendix*, Fig. S9) and maintained for 30 min. Then the soaking solution was removed and RH was slowly reduced to the optimal 96% (steps of 0.5%, 10-min equilibration period). A room-temperature (295 K) dataset was collected at this point, using a Mar345 detector coupled to the Rigaku MicroMax-007 rotating anode generator operating at 40 kV and 20 mA and equipped with Osmic confocal focusing optics. The dataset was processed with iMOSFLM and internally scaled with SCALA (*SI Appendix*, Table S1). Initial-difference maps that were calculated as described above, showed a strong peak of extra electron density (4 σ level), corresponding to one Ca^{2+} ion bound to the calcium-binding pocket of the C2A domain.

ACKNOWLEDGMENTS. We thank Arnau Casañas for revising the manuscript and the Plataforma Automatizada de Cristallografia (Barcelona) for technical assistance in the initial crystallization screenings and in the use of the FMS. Work in Barcelona was supported by Grant BIO2011-24333 [Ministerio de Economía y Competitividad (MINECO), Spain-Fondo Europeo de Desarrollo Regional (FEDER)] and work in Murcia by Grants BFU2011-22828 (MINECO, Spain-FEDER) and 08700/PI/08 (Fundación Seneca, Region de Murcia). X-ray data were collected at the European Synchrotron Radiation Facility Grenoble, France (beam line ID23.1) within a Block Allocation Group (Barcelona) and at the SOLEIL (beamline Proxima) Gives-sur-Yvette, France. C.F.-O. is recipient of a Junta para la Amplificación de Estudios postdoctoral contract from Consejo Superior de Investigaciones Cientificas-Fondo Social Europeo. J.G. is recipient of a Juan de la Cierva postdoctoral contract from MINECO.

1. Nalefski EA, Falke JJ (1996) The C2 domain calcium-binding motif: Structural and functional diversity. *Protein Sci* 5(12):2375–2390.
2. Rizo J, Südhof TC (1998) C2-domains, structure and function of a universal Ca2+-binding domain. *J Biol Chem* 273(26):15879–15882.
3. Cho W, Stahelin RV (2006) Membrane binding and subcellular targeting of C2 domains. *Biochim Biophys Acta* 1761(8):838–849.
4. Corbalán-García S, Gómez-Fernández JC (2006) Protein kinase C regulatory domains: The art of decoding many different signals in membranes. *Biochim Biophys Acta* 1761(7):633–654.
5. Shao X, Davletov BA, Sutton RB, Südhof TC, Rizo J (1996) Bipartite Ca2+-binding motif in C2 domains of synaptotagmin and protein kinase C. *Science* 273(5272):248–251.
6. Perisic O, Fong S, Lynch DE, Bycroft M, Williams RL (1998) Crystal structure of a calcium-phospholipid binding domain from cytosolic phospholipase A2. *J Biol Chem* 273(3):1596–1604.
7. Verdaguer N, Corbalan-Garcia S, Ochoa WF, Fita I, Gómez-Fernández JC (1999) Ca(2+) bridges the C2 membrane-binding domain of protein kinase Calpha directly to phosphatidylserine. *EMBO J* 18(22):6329–6338.
8. Xu GY, et al. (1998) Solution structure and membrane interactions of the C2 domain of cytosolic phospholipase A2. *J Mol Biol* 280(3):485–500.
9. Ochoa WF, et al. (2002) Additional binding sites for anionic phospholipids and calcium ions in the crystal structures of complexes of the C2 domain of protein kinase calpha. *J Mol Biol* 320(2):277–291.
10. Guerrero-Valero M, et al. (2009) Structural and mechanistic insights into the association of PKCalpha-C2 domain to PtdIns(4,5)P2. *Proc Natl Acad Sci USA* 106(16):6603–6607.
11. Marín-Vicente C, Gómez-Fernández JC, Corbalán-García S (2005) The ATP-dependent membrane localization of protein kinase Calpha is regulated by Ca2+ influx and phosphatidylinositol 4,5-bisphosphate in differentiated PC12 cells. *Mol Biol Cell* 16(6):2848–2861.
12. Marín-Vicente C, Nicolás FE, Gómez-Fernández JC, Corbalán-García S (2008) The PtdIns(4,5)P2 ligand itself influences the localization of PKCalpha in the plasma membrane of intact living cells. *J Mol Biol* 377(4):1038–1052.
13. Evans JH, Murray D, Leslie CC, Falke JJ (2006) Specific translocation of protein kinase Calpha to the plasma membrane requires both Ca2+ and PIP2 recognition by its C2 domain. *Mol Biol Cell* 17(1):56–66.
14. Corbin JA, Evans JH, Landgraf KE, Falke JJ (2007) Mechanism of specific membrane targeting by C2 domains: localized pools of target lipids enhance Ca2+ affinity. *Biochemistry* 46(14):4322–4336.
15. Manna D, et al. (2008) Differential roles of phosphatidylserine, PtdIns(4,5)P2, and PtdIns(3,4,5)P3 in plasma membrane targeting of C2 domains. Molecular dynamics simulation, membrane binding, and cell translocation studies of the PKCalpha C2 domain. *J Biol Chem* 283(38):26047–26058.
16. Fukuda M, Kojima T, Aruga J, Niinobe M, Mikoshiba K (1995) Functional diversity of C2 domains of synaptotagmin family. Mutational analysis of inositol high polyphosphate binding domain. *J Biol Chem* 270(44):26523–26527.
17. Schiavo G, Gu QM, Prestwich GD, Söllner TH, Rothman JE (1996) Calcium-dependent switching of the specificity of phosphoinositide binding to synaptotagmin. *Proc Natl Acad Sci USA* 93(23):13327–13332.
18. Bolsover SR, Gomez-Fernandez JC, Corbalan-Garcia S (2003) Role of the Ca2+/phosphatidylserine binding region of the C2 domain in the translocation of protein kinase Calpha to the plasma membrane. *J Biol Chem* 278(12):10282–10290.
19. Araç D, et al. (2006) Close membrane-membrane proximity induced by Ca(2+)-dependent multivalent binding of synaptotagmin-1 to phospholipids. *Nat Struct Mol Biol* 13(3):209–217.
20. Bai J, Chapman ER (2004) The C2 domains of synaptotagmin—partners in exocytosis. *Trends Biochem Sci* 29(3):143–151.
21. Lee H-K, et al. (2010) Dynamic Ca2+-dependent stimulation of vesicle fusion by membrane-anchored synaptotagmin 1. *Science* 328(5979):760–763.
22. van den Bogaart G, Meyenberg K, Diederichsen U, Jahn R (2012) Phosphatidylinositol 4,5-bisphosphate increases Ca2+ affinity of synaptotagmin-1 by 40-fold. *J Biol Chem* 287(20):16447–16453.
23. Di Paolo G, De Camilli P (2006) Phosphoinositides in cell regulation and membrane dynamics. *Nature* 443(7112):651–657.
24. Zhang X, Rizo J, Südhof TC (1998) Mechanism of phospholipid binding by the C2A-domain of synaptotagmin I. *Biochemistry* 37(36):12395–12403.
25. Chung SH, et al. (1998) The C2 domains of Rabphilin3A specifically bind phosphatidylinositol 4,5-bisphosphate containing vesicles in a Ca2+-dependent manner. In vitro characteristics and possible significance. *J Biol Chem* 273(17):10240–10248.
26. Ubach J, García J, Nittler MP, Südhof TC, Rizo J (1999) Structure of the Janus-faced C2B domain of rabphilin. *Nat Cell Biol* 1(2):106–112.
27. Coudevylle N, Montaville P, Leonov A, Zweckstetter M, Becker S (2008) Structural determinants for Ca2+ and phosphatidylinositol 4,5-bisphosphate binding by the C2A domain of rabphilin-3A. *J Biol Chem* 283(51):35918–35928.
28. Montaville P, et al. (2008) The PIP2 binding mode of the C2 domains of rabphilin-3A. *Protein Sci* 17(6):1025–1034.
29. Biadene M, Montaville P, Sheldrick GM, Becker S (2006) Structure of the C2A domain of rabphilin-3A. *Acta Crystallogr D Biol Crystallogr* 62(Pt 7):793–799.
30. Ubach J, et al. (2001) The C2B domain of synaptotagmin I is a Ca2+-binding module. *Biochemistry* 40(20):5854–5860.
31. Kiefersauer RTM, et al. (2000) A novel free-mounting system for protein crystals: Transformation and improvement of diffraction power by accurately controlled humidity changes. *J Appl Cryst* 33:1223–1230.
32. Friedrich R, Yeheskel A, Ashery U (2010) DOC2B, C2 domains, and calcium: A tale of intricate interactions. *Mol Neurobiol* 41(1):42–51.
33. Sutton RB, Davletov BA, Berghuis AM, Südhof TC, Sprang SR (1995) Structure of the first C2 domain of synaptotagmin I: A novel Ca2+/phospholipid-binding fold. *Cell* 80(6):929–938.
34. Fukuda M (2008) Regulation of secretory vesicle traffic by Rab small GTPases. *Cell Mol Life Sci* 65(18):2801–2813.
35. Pavlos NJ, Jahn R (2011) Distinct yet overlapping roles of Rab GTPases on synaptic vesicles. *Small GTPases* 2(2):77–81.
36. Stahl B, Chou JH, Li C, Südhof TC, Jahn R (1996) Rab3 reversibly recruits rabphilin to synaptic vesicles by a mechanism analogous to raf recruitment by ras. *EMBO J* 15(8):1799–1809.
37. Deák F, et al. (2006) Rabphilin regulates SNARE-dependent re-priming of synaptic vesicles for fusion. *EMBO J* 25(12):2856–2866.
38. Groffen AJ, et al. (2010) Doc2b is a high-affinity Ca2+ sensor for spontaneous neurotransmitter release. *Science* 327(5973):1614–1618.
39. Pang ZP, et al. (2011) Doc2 supports spontaneous synaptic transmission by a Ca(2+)-independent mechanism. *Neuron* 70(2):244–251.
40. Yao J, Gaffaney JD, Kwon SE, Chapman ER (2011) Doc2 is a Ca2+ sensor required for asynchronous neurotransmitter release. *Cell* 147(3):666–677.
41. Sánchez-Bautista S, Marín-Vicente C, Gómez-Fernández JC, Corbalán-García S (2006) The C2 domain of PKCalpha is a Ca2+-dependent PtdIns(4,5)P2 sensing domain: A new insight into an old pathway. *J Mol Biol* 362(5):901–914.
42. Guerrero-Valero M, Marín-Vicente C, Gómez-Fernández JC, Corbalán-García S (2007) The C2 domains of classical PKCs are specific PtdIns(4,5)P2-sensing domains with different affinities for membrane binding. *J Mol Biol* 371(3):608–621.
43. van den Bogaart G, et al. (2011) Synaptotagmin-1 may be a distance regulator acting upstream of SNARE nucleation. *Nat Struct Mol Biol* 18(7):805–812.
44. Fernandez I, et al. (2001) Three-dimensional structure of the synaptotagmin 1 C2B-domain: Synaptotagmin 1 as a phospholipid binding machine. *Neuron* 32(6):1057–1069.
45. Xue M, Ma C, Craig TK, Rosenmund C, Rizo J (2008) The Janus-faced nature of the C(2)B domain is fundamental for synaptotagmin-1 function. *Nat Struct Mol Biol* 15(11):1160–1168.
46. Seven AB, Brewer KD, Shi L, Jiang QX, Rizo J (2013) Prevalent mechanism of membrane bridging by synaptotagmin-1. *Proc Natl Acad Sci USA* 110(34):E3243–E3252.
47. Kuo W, Herrick DZ, Cafiso DS (2011) Phosphatidylinositol 4,5-bisphosphate alters synaptotagmin 1 membrane docking and drives opposing bilayers closer together. *Biochemistry* 50(13):2633–2641.
48. Honigmann A, et al. (2013) Phosphatidylinositol 4,5-bisphosphate clusters act as molecular beacons for vesicle recruitment. *Nat Struct Mol Biol* 20(6):679–686.
49. Ausili A, Corbalán-García S, Gómez-Fernández JC, Marsh D (2011) Membrane docking of the C2 domain from protein kinase Cα as seen by polarized ATR-IR. The role of PIP_2. *Biochim Biophys Acta* 1808(3):684–695.
50. Landgraf KE, Malmberg NJ, Falke JJ (2008) Effect of PIP2 binding on the membrane docking geometry of PKC alpha C2 domain: An EPR site-directed spin-labeling and relaxation study. *Biochemistry* 47(32):8301–8316.
51. Lai CL, Landgraf KE, Voth GA, Falke JJ (2010) Membrane docking geometry and target lipid stoichiometry of membrane-bound PKCα C2 domain: A combined molecular dynamics and experimental study. *J Mol Biol* 402(2):301–310.
52. Russi S, et al. (2011) Inducing phase changes in crystals of macromolecules: Status and perspectives for controlled crystal dehydration. *J Struct Biol* 175(2):236–243.